# Pyroelectric energy harvesting from power electronic substrates

Mohammad Nia, Ali; Rezaniakolaei, Alireza

*Published in:*
Energy Conversion and Management

*DOI (link to publication from Publisher):*
10.1016/j.enconman.2023.117233



*Publication date:*
2023

*Document Version*
Publisher's PDF, also known as Version of record

Energy Conversion and Management 290 (2023) 117233

Contents lists available at ScienceDirect

Energy Conversion and Management

journal homepage: www.elsevier.com/locate/enconman

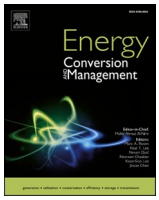

# Pyroelectric energy harvesting from power electronic substrates

Ali Mohammadnia, Alireza Rezania *

*AAU Energy, Aalborg University, Pontoppidanstræde 111, DK-9220 Aalborg, Denmark*

ARTICLE INFO

*Keywords:*
Pyroelectricity
Power electronic substrate
Energy harvesting
Thermal management
Self-powered sensors
Dynamic modelling

ABSTRACT

Energy harvesting from available resources can lead to implementation of more controlling and actuating devices for industrial internet of things (IIoT). Energy harvesting from temperature fluctuations in power electronic devices by pyroelectric materials is a key solution to achieve self-powered sensor systems. In this study, performance of a pyroelectric energy harvester (PEH), utilized as a dielectric substrate in power electronic modules, is investigated. Accordingly, a comprehensive analytical model is developed in MATLAB software, and the theoretical results are validated with experimental data. The results of this study show that, the pyroelectric substrate can harvest an average power of 50 μW/cm$^2$. Effect of amplitude and frequency of input heat, cooling density, and load resistance over PEH are studied. The results reveal that, frequency of the input heat rate higher than 2 Hz does not have a sensible impact on the power generation by the pyroelectric module. Convective cooling density with low heat transfer coefficients led to higher power generation. On the contrary, it can cause operating at higher temperature than the Curie temperature. The energy harvesting concept developed, for the first time, in this study shows significant potential of pyroelectric direct bonded copper substrate to provide self-powered sensors for IIoT in a vast range of power electronic applications.

## 1. Introduction

It is known that a fraction of energy flow wastes as heat in power electronic devices with semiconductor chips such as diodes, insulated-gate bipolar transistors, etc. Operating under a high electrical field with small chip area can result in high-temperature fluctuations in these devices. The high-temperature oscillations reduce durability and lifetime of the power electronic devices. Therefore, reliable sensors network is desired to support industrial internet of things (IIoT) for refining and optimizing the process controls. These sensor platforms, however, need an electrical energy supply. Harvesting the thermal energy available in power semiconductor devices allows for supporting more sensors and monitoring components in different parts of the system for intelligent control.

Materials used commonly for thermal energy harvesting are thermoelectric materials. These semiconductor-based energy materials generate electrical power when a temperature difference is created across the material. Thermoelectric devices have various advantages such as long lifespan, low maintenance, no moving parts, and compact structure [1]. These devices have been used for energy harvesting [2,3], thermal management[4], hybrid energy systems [5], etc. However, low conversion efficiency and dependency on high-temperature differences for delivering suitable power are drawbacks within this energy harvesting technology.

Pyroelectric materials, on the other hand, are alternative energy materials that provide electrical potential by rate of temperature changes [6]. Pyroelectricity can provide effective power at lower operating temperatures with only temperature fluctuations. Most studies in the field of pyroelectricity have focused on development of efficient materials with improved pyroelectric properties. Wang et al. [7] investigated a high-performance pyroelectric ceramic composite with doping of 0.1 wt% hexagonal boron nitride and achieved power generation of 8.46 μW in a disk with a diameter of 10 mm. Patel and Novak [8] studied antiferroelectric ceramics as high energy–density pyroelectric materials and obtained a large energy density of 1.0 MJ/m$^3$ per cycle with operating temperature fluctuating between 303 K and 403 K and with electric fields of 1 and 9 kV/mm based on the phase transition of the material.

Nevertheless, pyroelectric energy harvesting applications are designed to show practical aspects of nature of the developed materials [9]. Yu et al. [10] developed a transparent pyroelectric energy harvester (PEH) combined with phase change materials, where sunlight could pass across the transparent pyroelectric material. The phase change material placed behind PEH was used to provide optimal temperature fluctuations during the periodic solar irradiation. Wang et al. [11] developed a

* Corresponding author.
*E-mail address:* alr@energy.aau.dk (A. Rezania).

https://doi.org/10.1016/j.enconman.2023.117233
Received 5 February 2023; Received in revised form 25 May 2023; Accepted 28 May 2023
Available online 4 June 2023

**Nomenclature**

| | |
|---|---|
| $A$ | area, [$m^2$] |
| $c$ | volumetric heat capacity, [$J/m^3K$] |
| $C$ | capacitance, [F] |
| $D$ | electrical displacement, [$C/m^2$] |
| $E$ | electric field [V/m] |
| $h$ | heat transfer coefficient, [$W/m^2K^1$] |
| $h_{pyro}$ | height of pyroelectric material, [m] |
| $i$ | current, [A] |
| $k$ | thermal conductivity, [W/mK] |
| $L$ | length, [m] |
| $P$ | power, [W] |
| $p$ | pyroelectric coefficient, [$C/m^2K$] |
| $R$ | electrical resistance, [Ω] |
| $T$ | temperature, [K] |
| $t$ | time, [s] |
| $V$ | voltage, [V] and volume, [m3] |
| $X$ | strain |
| $x$ | stress [$N/m^2$] |

*Greek symbol*

| | |
|---|---|
| $\varepsilon$ | emissivity |
| $\varepsilon_{pyro}$ | dielectric permittivity [F/m] |
| $\rho$ | density, [$kg/m^3$] |
| $\sigma$ | Stefan–Boltzmann constant, [$W/m^2K^4$] |

*Subscript and Superscript*

| | |
|---|---|
| *amb* | ambient |
| *cond* | conduction |
| *conv* | convection |
| *load* | load |
| *i* | 1,2,3,4,5,6 |
| *in* | input |
| *m* | 1,2,3 |
| *oc* | open-circuit |
| *out* | output |
| *pyro* | pyroelectric |
| *rad* | radiation |
| *up* | up side |

solar-induced pyroelectric nanogenerator with strong solar thermal and superior solar radiation absorption and conversion. Their PEH provided a maximum temperature change rate of 14.3 °C/s under sunlight irradiation with 33.4 mHz frequency and generated 1.5 $mW/m^2$ output power. Yu et al. [12] proposed an advanced PEH using phase change material composite. The system controlled the temperature fluctuations effectively and provided stable output power. Kim et al. [13] studied a novel electro-thermodynamic energy harvesting cycle applied to temperature fluctuations of automotive exhaust gas by pyroelectric material and investigated domain structure of the material to optimize performance of the suggested energy harvesting cycle. Xue et al. [14] designed and fabricated a wearable pyroelectric nanogenerator in a respirator for energy harvesting from human breathing. Their thin-film device showed promising potential to provide self-powered multifunctional wearable applications with maximum power delivery of 8.31 μW at temperature difference of 5 °C with ambient temperature. Lee et al. [15,16] developed a highly stretchable hybrid nanogenerator with combined piezo- and pyro-electric properties to harvest both kinetic and thermal energy of the human body. Their device exhibited high robustness even after stretching by 30% and provided stable hybrid output power.

Zebek et al. [17] employed natural oscillations of a two-phase working fluid in heat pipes to drive power from a change in surface charge in pyroelectric materials. Using lead zirconate titanate and lead magnesium niobate-lead titanate materials, open circuit voltage of 0.4 V and 0.8 V, respectively, was generated with a temperature oscillation range between 0.1 K and 5 K at frequency of 0.45 Hz. Raouadi and Touayar [18] enhanced pyroelectric energy harvesting from wind using a vortex generator mechanism. They reported 0.109 $\mu A/cm^2$ output current and 2.82 $\mu W/cm^2$ peak power density at 25 m/s wind velocity with a 9 μm thickness polyvinylidene fluoride film. Tabbai et al. [19] investigated harvesting thermal energy loss in a disc brake pad. They predicted proper time to change the brake pad by monitoring magnitudes of energy harvesting density and voltage generation as functions of pad thicknesses, speed of the vehicle, and temperature traversed by the pyroelectric material. Lheritier et al. [20] developed a macroscopic PEH with multilayer capacitors to reach 40% of the Carnot efficiency at a temperature difference of 10 K.

Pyroelectric materials exhibit ferroelectricity and have proper thermal conditions for hybrid energy generation with piezoelectric and thermoelectric energy harvesters, respectively. Kang and Yeatman [21] proposed a hybrid energy harvesting concept to exploit both pyro- and piezo-electric phenomena simultaneously. The prototype provided 0.4 μW at 15 K temperature difference and frequency of 0.02 Hz. Zhang et al. [22] developed a novel wearable solar-driven pyro-thermo-electric hybrid energy harvester. Their novel energy harvester was able to harvest both static temperature gradients and dynamic temperature fluctuations. The hybrid energy harvester could successfully charge two commercial capacitors to a sum voltage of 3.7 V in 800 s under illumination intensity of 1500 $W/m^2$.

The literature in the field of pyroelectricity shows the high potential of this material for energy harvesting from thermal energy systems. Power electronic devices have been extremely used in many high-technology applications with a wide range of operating temperatures. Self-powered condition monitoring systems can enhance reliability and safety of these devices. In this study, a feasibility assessment of pyroelectric energy harvesting from temperature fluctuations of power electronic components is investigated for the first time. In this approach, PEH is applied as the direct bonded copper (DBC) substrate that is commonly used in power electronic modules. DBCs are consisted of a ceramic material plate with copper sheets bonded to the sides. The bottom layer of the DBC is then soldered to a heat spreader, with specific cooling performance, in power electronic systems. Dielectric properties of a PEH and its similar structure to the DBCs make it a substantial alternative for DBCs while the conceptual PEH produces electrical energy from temperature oscillations in the power electronics for sensor platforms, condition monitoring, and wireless communications. Since power electronic modules with high heat density rates and temperature fluctuations are widely used in power systems and renewable energy systems, feasibility study of the energy harvesting concept proposed in this work can open a window of opportunity toward future self-powering and autonomous IIoT applications.

## 2. Pyroelectric energy harvester

Pyroelectric materials are dielectric and can be polarized by a rate of change in temperature that makes electrical displacements due to non-centrosymmetric crystal shape. Spontaneous polarization in the materials' dipoles leads to surface polarization in the pyroelectric substance, as can be seen in Fig. 1a. According to the charge storage capacity of the pyroelectric material, there is no electrical current flow in the created circuit. The heating process, Fig. 1b, creates disarray in the material dipoles and reduces the spontaneous polarization of the pyroelectric substances. The reduction in spontaneous polarization is shown by shorter arrow length which leads to ejecting electrons from the material

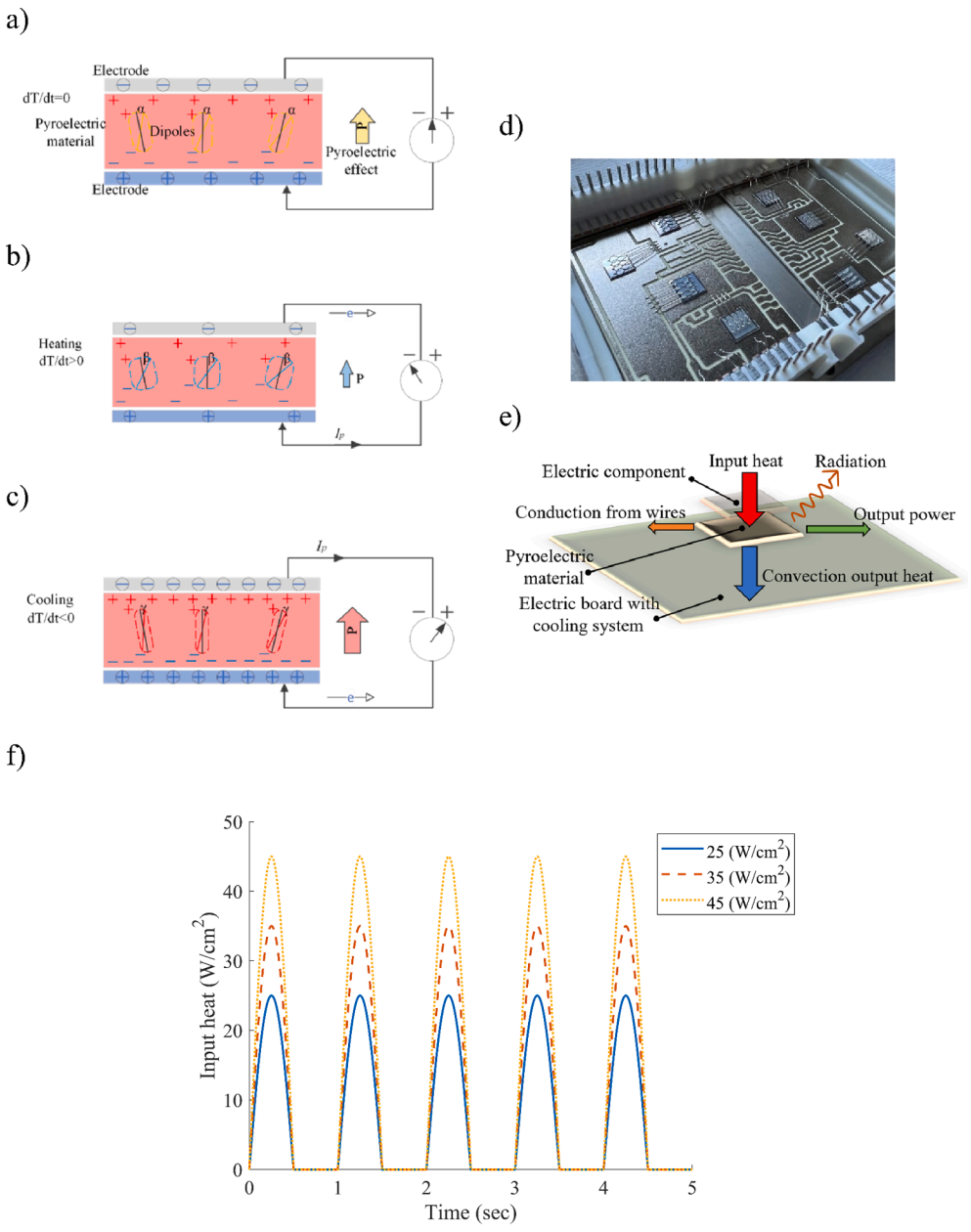


**Fig. 1.** (a, b, and c) schematic diagrams from electrical current generation by pyroelectric materials, d) a photo image from a power electronic module, (e) energy flow diagram of a sample PEH, and (f) various input heat rates applied on PEH with frequency of 1 Hz.

surfaces in correspondence with charge capacity. The ejected electrons from the pyroelectric surfaces create a negative electrical current in the circuit. On the other hand, the cooling process, shown in Fig. 1c, increases arrangement of the material dipoles. Therefore, strong spontaneous polarization flows electrons in the positive direction of the circuit corresponding to the surface charge of PEH. The electrical current generation during the heating and cooling processes can be either utilized or stored. As a result, the temperature variation rate affects the polarization of the pyroelectric material and leads to electrical current in the circuit.

Pyroelectric materials are within a subset of piezoelectric materials and mechanical stress due to temperature change impacts the polarization of the substances. Therefore, two phenomena can influence the polarization of pyroelectric materials. The primary pyroelectric effect is oriented from the temperature variations in the pyroelectric materials under a constant mechanical strain preventing expansion or contraction. The secondary pyroelectric effect, which is orientated from the deformation of the pyroelectric substance, corresponds to the thermal strain of applied temperature variations. In addition, there is a tertiary pyroelectric or false effect that emerges in inhomogeneous heating or cooling processes and is an intrinsic property of piezoelectric materials [23].

The differential of electric displacement with independent temperature, electric field, and stress in a pyroelectric material can be explained as:

$$dD_m = \left(\frac{\partial D_m}{\partial x_i}\right)_{E,T} dx_i + \left(\frac{\partial D_m}{\partial E_n}\right)_{x,T} dE_n + \left(\frac{\partial D_m}{\partial T}\right)_{E,x} dT \quad (1)$$

where $D$, $x$, $E$, and $T$ are respectively the electric displacement, stress, electric field, and temperature of the pyroelectric material. Without an electric field or under a constant electric field, the electric displacement is a function of both stress and temperature, where strain in the material can be determined by these parameters. Thus:

$$dD_m = \left(\frac{\partial D_m}{\partial x_i}\right)_T dx_i + \left(\frac{\partial D_m}{\partial T}\right)_x dT \tag{2}$$

$$dx_i = \left(\frac{\partial x_i}{\partial X_j}\right)_T dX_j + \left(\frac{\partial x_i}{\partial T}\right)_X dT \tag{3}$$

where, $X$ is the strain and if $dX_j = 0$. By combining equations (2) and (3), the electric displacement is determined as:

$$dD_m = \left[\left(\frac{\partial D_m}{\partial x_i}\right)_T \left(\frac{\partial x_i}{\partial T}\right)_X + \left(\frac{\partial D_m}{\partial T}\right)_x\right] dT \tag{4}$$

To represent the overall pyroelectric coefficient, equation (4) can be rearranged as follows:

$$\left(\frac{dD_m}{dT}\right)_X = \left(\frac{\partial D_m}{\partial T}\right)_x + \left(\frac{\partial D_m}{\partial x_i}\right)_T \left(\frac{\partial x_i}{\partial T}\right)_X \tag{5}$$

where the first and second terms on the right-hand side of the equation refer to the primary and secondary effects of a pyroelectric material, respectively. The pyroelectric current undergoing heating or cooling processes can be determined as follows [24–26]:

$$i_{pyro} = Ap\frac{dT}{dt} \tag{6}$$

where $A$, $p$, and $t$ represent area of the electrode surface, overall pyroelectric coefficient, and time, respectively. As can be deduced from equation (6), the slope of temperature variations in heating or cooling processes determines the current direction in the electrical circuit. The calculated current by this equation refers to the pyroelectric short-circuit current. Moreover, the open-circuit voltage can be given as follows [27–30]:

$$V_{oc} = \frac{ph_{pyro}}{\varepsilon_{pyro}}\Delta T \tag{7}$$

where, $h_{pyro}$ and $\varepsilon_{pyro}$ refer to PEH thickness and dielectric permittivity, respectively. Equations (6) and (7) show that, the short-circuit current is a function of area of the pyroelectric, while the open-circuit voltage depends on thickness of PEH.

## 3. Energy harvesting characterization

The pyroelectric energy generation concept in this study is based on temperature oscillations in power electronic semiconductor chips due to modular frequency. Fig. 1d shows a typical power electronic module with eight semiconductor chips soldered on a DBC substrate. The ceramic substrates in power electronic modules are used to thermally conduct heat generation to heatsink as well as to provide the interconnections and to form the electric circuit. To use PEH as an alternative for the DBC substrate, it is required to coat electrodes and add a dielectric layer on the electrode to prevent electrical leakage and avoid electrical conductivity of the substrate. Fig. 1e shows a schematic diagram of energy flow in PEH applied as the DBC substrate. Therefore, the energy balance equation for the pyroelectric module can be expressed as follows:

$$\rho cV\frac{dT}{dt} = \dot{Q}_{in} - \dot{Q}_{rad} - \dot{Q}_{conv} - \dot{Q}_{cond} - P_{pyro} \tag{8}$$

where, $\rho$, $c$, and $V$ refer to density, volumetric heat capacity, and volume of PEH, respectively. The $\dot{Q}_{in}$ is the input heat applied on the pyroelectric module by the semiconductor chip. This is determined as a critical parameter in design of an optimal PEH as half-sinusoid heat waves with different densities and frequencies. Fig. 1f shows the applied input heat rates with maximum values at 25, 35, and 45 W/cm$^2$ charge densities and frequency of 1 Hz. These input heat rates are selected to provide a wide range of temperature oscillations in PEH. Other reference values for main design parameters of PEH are shown in Table 1.

The radiation heat lost from upper side is calculated as follows:

**Table 1**
Reference values and design parameters of the pyroelectric PZT-5A energy harvester considered in the simulations.

| Parameter | Symbol | Value |
|---|---|---|
| Pyroelectric coefficient | $p$ | $-38 \times 10^{-5}$C/(m$^2$K) |
| Volume specific heat capacity of pyroelectric material | $c$ | $2.5 \times 10^6$ J/(m$^3$K) |
| Permittivity of pyroelectric material | $\varepsilon_{pyro}$ | $9.73 \times 10^{-9}$F/m |
| Pyroelectric density | $\rho$ | 7800 kg/m$^3$ |
| Emissivity of pyroelectric material | $\varepsilon$ | 0.8 |
| Stefan–Boltzmann constant | $\sigma$ | $5.67 \times 10^{-8}$ W/m$^2$K$^4$ |
| Pyroelectric area | $A$ | 1 cm$^2$ |
| Pyroelectric volume | $V$ | 1 cm × 1 cm × 0.05 cm |
| Pyroelectric thickness | $h_{pyro}$ | 0.5 mm |
| Ambient temperature | $T_{amb}$ | 21 ℃ |
| External load resistance | $R_{load}$ | 10000 Ω |
| Circuit wires diameter | $D_{wire}$ | 0.1 mm |
| Circuit wires length | $L_{wire}$ | 5 cm |
| Thermal conductivity of bonding wires | $k_{wire}$ | 386 W/(mK) |
| Input heat rate | $\dot{Q}_{in}$ | 35 W/(cm$^2$) |
| Input heat frequency | – | 1 Hz |
| Convection heat transfer coefficient | $h$ | 1000 W/(m$^2$K) |

$$\dot{Q}_{rad} = \varepsilon\sigma A\left(T_{up}^4 - T_{amb}^4\right) \tag{9}$$

where, $\varepsilon$, $T_{up}$, $\sigma$, and $T_{amb}$ are emissivity, temperature of the top surface, Stefan-Boltzmann constant, and ambient temperature, respectively. The $\dot{Q}_{conv}$ refers to forced convection heat transfer on the bottom side of PEH calculated as:

$$\dot{Q}_{conv} = hA\left(T_{pyro} - T_{amb}\right) \tag{10}$$

where, $h$ is the heat transfer coefficient assumed in wide range of 100, 1000, and 10,000 $W/(m^2K)$. Conductive heat loss from the wire bonds is calculated as follows:

$$\dot{Q}_{cond} = \frac{2k_{wire}A_{wire}}{L_{wire}}\left(T_{pyro} - T_{amb}\right) \tag{11}$$

where, $k$, $A$, and $L$ are thermal conductivity, cross-sectional area, and length of the electrical circuit wires. Eventually, $P_{pyro}$ is pyroelectric power generation calculated as follows:

$$P_{pyro} = \frac{(V_{out})^2}{R_{load}} \tag{12}$$

where, $R_{load}$ is external electrical load resistance, and $V_{out}$ is the output voltage of PEH connected to the load resistance and calculated according to the electrical circuit [28,30] as follows:

$$pA\frac{dT}{dt} = C_{pyro}\frac{dV_{out}}{dt} + \left(\frac{1}{R_{load}} + \frac{1}{R_{pyro}}\right)V_{out} \tag{13}$$

where, $C_{pyro}$ and $R_{pyro}$, respectively, represent pyroelectric capacitance and resistance.

In this study, convection heat loss from the top surface and natural convection from the wire bonds are neglected because of using insulation gel filler on top surface of the conventional power electronic modules. Moreover, it is assumed that the heating and cooling processes make uniform temperature in the pyroelectric material because of the low thickness of PEH. Size of the pyroelectric sample in this study is 10 mm × 10 mm with a thickness of 0.5 mm. Since the pyroelectric coefficient does not change significantly under the operating temperature conditions, this coefficient is assumed to be constant at $-38 \times 10^{-5}$C/(m$^2$K). Other main design parameters of the lead zirconate titanate (PZT-5A) energy harvester used in this study are listed in Table 1.

## 4. Time-step dependency of the solution

The transient governing equations for pyroelectric energy harvesting, coupled with the thermal and electrical conditions, are solved over a determined period by a developed model in MATLAB software. Therefore, the temperature iteration in each time zone and governing equations are converged during several time steps. Accuracy of the results is dependent to magnitude of the time steps; thus, pyroelectric energy harvesting is investigated at different time steps in this study. Table 2 shows average pyroelectric output voltage at different numbers of time steps during the operation period. To avoid large running-time and acceptable accuracy of the results, the 1500-timestep is selected as the reference value during the 5 s operating time.

## 5. Validation of the theoretical results

Pyroelectric material generates electrical power by rate of temperature change. Thus, an experimental verification is conducted to verify energy harvesting performance of the pyroelectric material used in the theoretical analysis. The theoretical power generation is compared to experimental results under the same temperature profile. The experimental setup comprises a two-layer pyroelectric PZT-5A energy harvester with a 63.5 mm × 31.3 mm area and thickness of 0.19 mm for each layer. The pyroelectric material is sandwiched between two copper plates with thickness of 0.5 mm to create a homogeneous temperature distribution over PEH. Two thermoelectric modules, with size of 30 mm × 30 mm, are used on each side of PEH to heat and cool the module frequently with certain frequencies. The TE modules are fixed between two copper sheets with 1 mm thickness. A natural convection air cooled heatsink is used on each side of PEH to transfer heat into the surrounding ambient. Fig. 2a shows the constructed experimental setup in this study and Fig. 2b demonstrates a schematic from exploded view of the setup components. As shown, PEH is sandwiched between copper sheets and thermoelectric modules. The thermoelectric modules heat up and cool down PEH and create temperature oscillations for energy harvesting. Copper sheets, with high thermal conductivity, help the creation of homogenous temperature on PEH. The electrical resistance connected to the pyroelectric circuit is, furthermore, shown in this figure. An OTG-PM fiber optic temperature sensor [31] was used to measure temperature variations on PEH. The fiber optic sensors are in contact with the center of PEH through the holes created across the setup. The voltage generation under electrical resistance and the corresponding temperature on PEH are measured simultaneously by the data acquisition device. Accordingly, the power generation by PEH is calculated. The output voltage of the temperature sensor device and the output voltage/current of PEH are recorded by a Keysight B2902A unit [32]. Then a square signal with a certain frequency and amplitude was applied to the thermoelectric modules to provide temperature variations.

The temperature variation measured in the experiments is used as input temperature in the simulation for validation. Furthermore, the properties of the commercial PEH are defined as design parameters in the analytical investigation. Fig. 2c shows a comparison between the theoretical and experimental output voltage under a 506.3 kΩ load resistance. Since the measured temperature contains fluctuations, a curve is fitted for temperature of PEH and used as the input of the analytical model, as shown in Fig. 2c. There is a phase difference between the variation of the temperatures and output voltage. This is a result of the external load on the pyroelectric voltage. According to equations (6) and (7), the short-circuit current is a function of the rate of temperature variation while the open-circuit voltage is a function of temperature variation. The short-circuit current is zero at the peak points of the temperature profile, but the open-circuit voltage is at extremum values at the peak points of the temperature profile. Therefore, there is a 90-degree phase difference between short-circuit current (full-load condition) and open-circuit voltage (no-load condition) according to temperature variations. Since the load resistance connected to PEH applies a significant load compared to the internal load of PEH module, the phase of the output voltages is closer to the full-load

**Table 2**
Convergency of the pyroelectric output voltage during a 5-sec operation time.

| Number of time steps during 5 sec | Average of Pyroelectric output voltage (mV) | Percentage of change in each step (%) |
|---|---|---|
| 200 | −2.0 | – |
| 400 | −3.4 | 70 |
| 600 | −4.5 | 32.35 |
| 1000 | −6.0 | 25 |
| 1500 | −6.6 | 10 |
| 2000 | −6.6 | 0 |

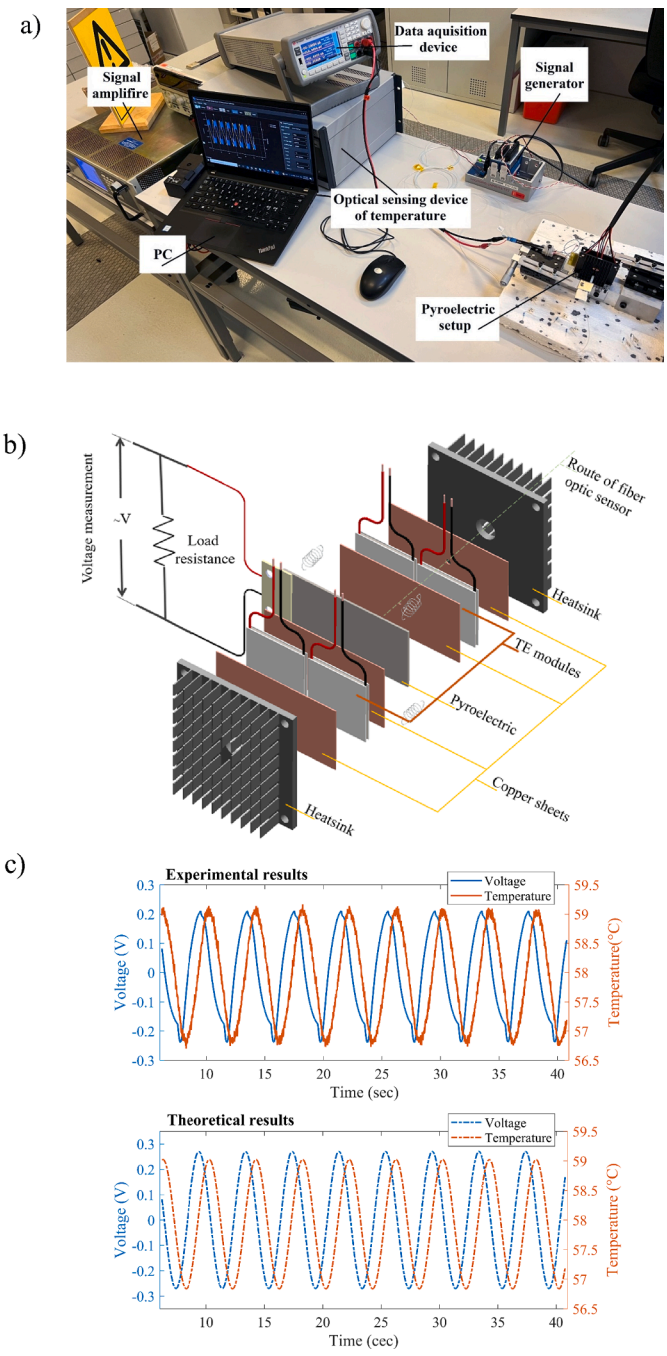


**Fig. 2.** (a) experimental setup, (b) an exploded view from setup components, and (c) comparison between theoretical and experimental output voltage of PEH.

condition. Particularly, the applied load on PEH results in zero voltage at temperature peak points close to the full-load condition. It is noteworthy that, for a specific resistance, the voltage and current have a same phase according to Ohm's law. Furthermore, according to the experimental output voltage profile, there is a clear non-linearity in the pyroelectric property of the material that is not considered in our theoretical analysis. The biggest deviations between the theoretical results are at the peak points of the voltages. The peak-to-peak deviation of the theoretical results is 15.1% while the average deviation is less than this value.

Standard deviations of 20 data points recorded for temperature and voltage are calculated using equations (14) and (15) [33]. The deviations are $\pm$ 9.251 $\times$ $10^{-2}$ ℃ and $\pm$ 3.831 $\times$ $10^{-3}$ V for pyroelectric temperature and voltage, respectively. Consequently, the uncertainties for voltage and temperature are estimated at approximately 1.8% and 0.16%, respectively.

$$Sx = \left[\frac{1}{N-1}\sum_{i=1}^{N}(X_i - \overline{X})^2\right]^{\frac{1}{2}} \tag{14}$$

$$\overline{X} = \frac{1}{N}\sum_{i=1}^{N} X_i \tag{15}$$

## 6. Results and discussion

In this section, the effect of critical design parameters on performance of PEH is discussed. The response of pyroelectric material is reported parametrically while the rest of parameters are kept constant at their reference values as mentioned in Table 1. Fig. 3 shows the variation of temperature, output voltage, output current, and power generation of PEH at various input heat rates. As shown in Fig. 3a, the higher input heat rates lead to larger temperature variation rates. Consequently, higher temperature difference and the derivative of the temperature with respect to time cause generating higher pyroelectric voltage and current, as can be seen in Fig. 3b and Fig. 3c. It is noteworthy that, different thermal boundary conditions with the boundary conditions imposed in the experimental validation caused different and asymmetric voltage signals. During the transient operation of PEH, there are two major phenomena related to its temperature variation. First, increasing the energy material temperature during the beginning of the operation time and next, higher cooling rates due to its temperature increment. Increasing the temperature at the beginning of the heating process results in a higher voltage and current generation rate. Since power is a multiplication of voltage and current, this phenomenon is magnified in the power peak in Fig. 3d. At these peaks, because the pyroelectric material is not at its peak temperatures, level of the voltage and current generation is low during the cooling process. Besides, when the temperature of the pyroelectric material increases, higher temperature variation accurs during the cooling process. This trend can be seen as higher positive voltage and current in the absence of the power and as higher power generation after the peak power points. It is worth to note that, there is no rectifier in the presented electrical circuit, therefore the negative voltages and currents are emerging in Fig. 3.

The transient temperature response of PEH under different input heat rate frequencies is shown in Fig. 4a. As can be seen, lower frequencies lead to higher temperature amplitudes. Contrariwise, the higher frequencies lead to smaller temperature oscillations. However, since PEH generates power by rate of the temperature variations, higher temperature variation does not make higher voltage. For instance, temperature variations at 0.2 Hz frequency create 200 K temperature oscillation, and 1 Hz input heat rate frequency creates 50 K temperature oscillation. Nevertheless, by comparison of the output voltages, Fig. 4b shows that operating under higher frequencies provides higher voltages than a PEH working under lower frequencies. Fig. 4c-e illustrates the output voltages at frequencies of 2, 5, and 10 Hz.

The power harvested at 0.2, 0.6, and 1 Hz input heat frequencies in Fig. 5a shows that, the higher frequencies lead to higher power generation. The pyroelectric power generated at 2, 5, and 10 Hz input heat rate frequencies are, furthermore, shown in Fig. 5b-d. Although higher input heat rate frequencies lead to higher power peak points, the power generation width becomes narrower. Thus, to estimate the energy harvesting, average value of the output power generation versus frequency is shown in Fig. 5e. The average output power is calculated as:

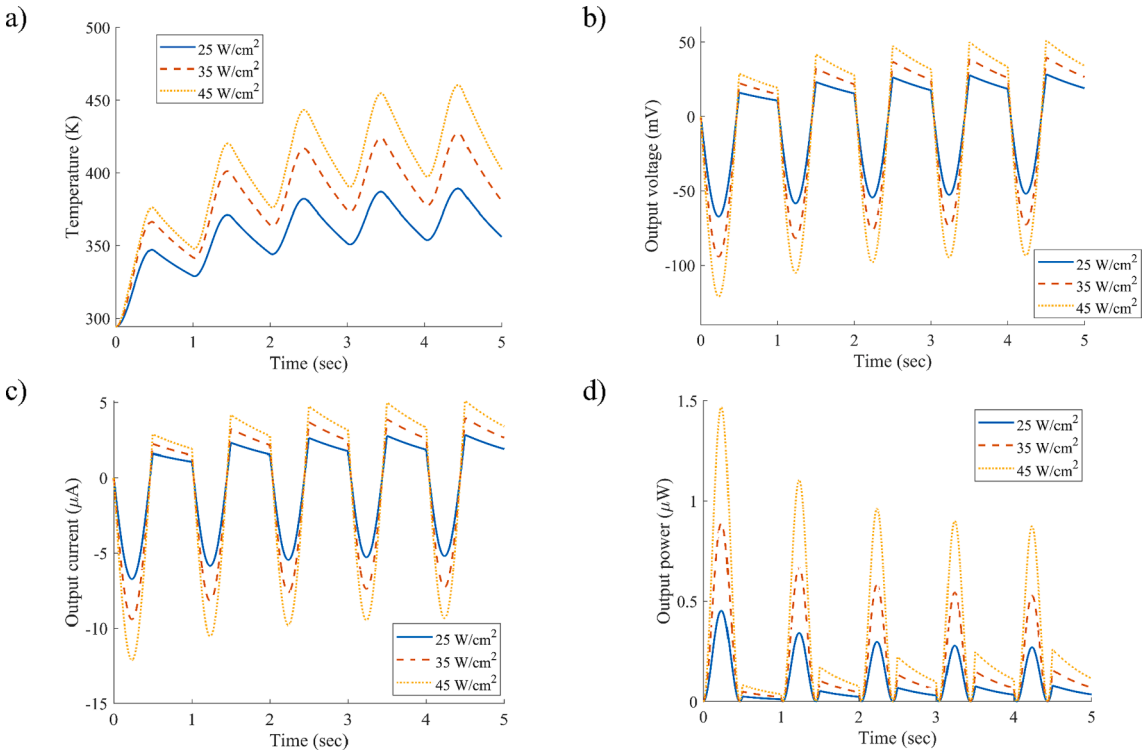


**Fig. 3.** Transient (a) pyroelectric temperature, (b) output voltage, (c) output current, and (d) output power at various input heat rates.

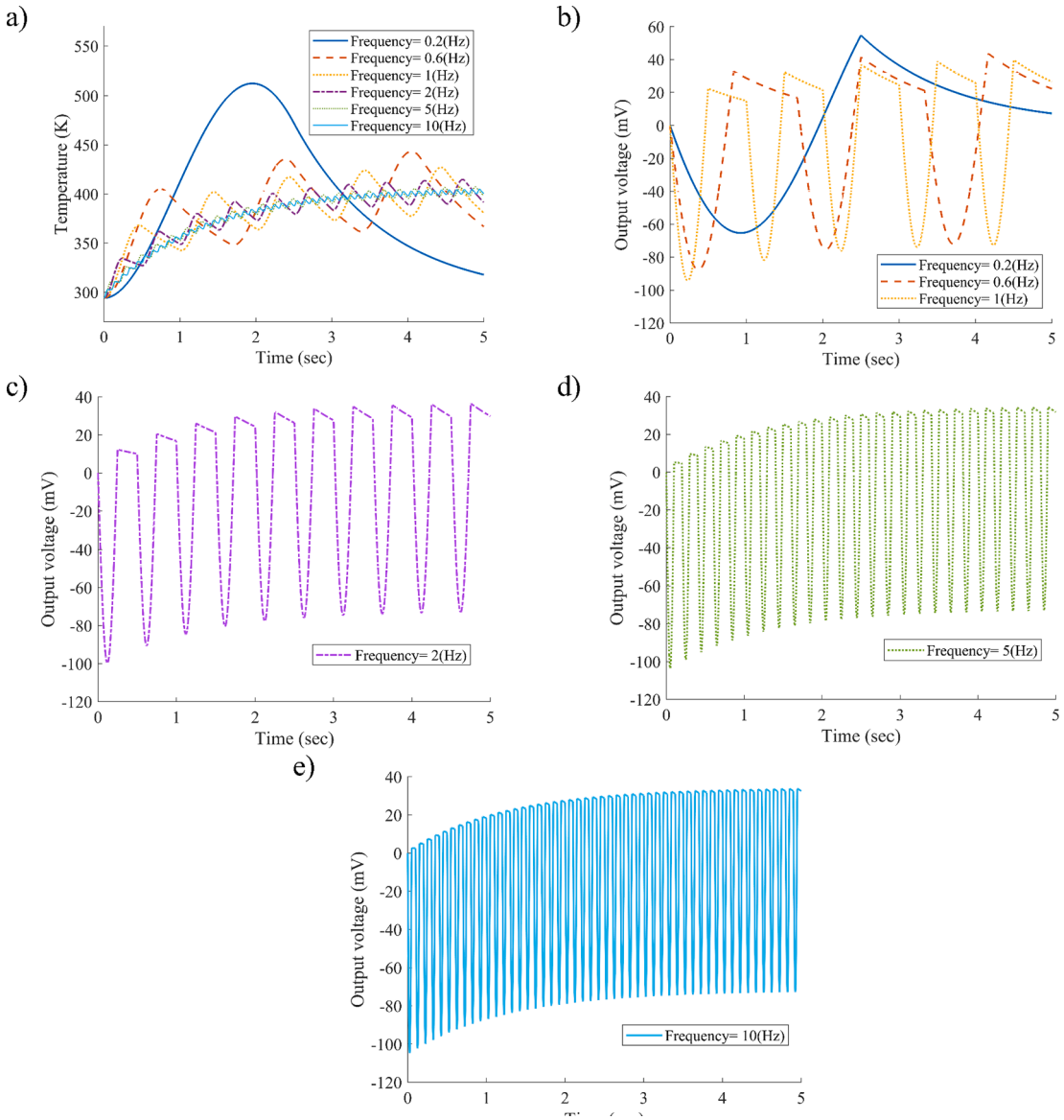


**Fig. 4.** (a) Temperature variations of PEH at different frequencies; and output voltage at input heat rate frequencies of (b) 0.2, 0.6, and 1 Hz, (c) 2 Hz, (d), 5 Hz, and (e) 10 Hz.

$$P_{ave} = \frac{1}{N}\sum_{i=1}^{N} P_i \tag{16}$$

$N$ is the number of calculated transient power calculated during 10 s, and $P_i$ is the amount of calculated transient power for the corresponding points.

As shown, the average power generation by PEH reaches its maximum at a frequency of 2.4 Hz under the applied input heat fluxes. After this operating frequency, there is convexity on the average power curve due to the transient response of PEH during operating cycles as a response to temperature oscillations. Another parameter with major effect on PEH performance is the heat transfer coefficient on the cold side of PEH provided by the cooling fluid. Fig. 6a shows the temperature variation of PEH at different heat transfer coefficients. Three values are selected in this simulation to represent vast types of cooling processes, namely 100 W/m$^2$K for forced air cooling, 1,000 W/m$^2$K for single-phase liquid cooling, and 10,000 W/m$^2$K for two-phase heat transfer processes. As shown, the low heat transfer coefficient is not sufficient to reject the input heat. Thus, the temperature of PEH increased gradually higher than the Curie temperature of the pyroelectric material. The Curie temperature of PZT-5A in this study is approximately 623 K. At this temperature, the material loses its pyroelectric properties and is not capable of proper power generation. It is therefore necessary to define a low limit point for the heat transfer coefficient in PEH systems under full-load operating conditions. Under the 45 W/cm$^2$ input heat rate density, the critical heat transfer is approximately 480 W/m$^2$K in this study.

At 1,000 W/m$^2$K, the mean operating temperature of PEH after reaching the stable periodic temperature oscillation is 370 K. In this stage, the heating and cooling processes are balanced in each thermal cycle with effective temperature oscillation created on PEH. Moreover, at 10,000 W/m$^2$K, the cooling rate is the most dominant parameter, where the heating process is unable to create temperature oscillations sufficient for significant power generation. Thus, the mean temperature of PEH decreases dramatically, and the periodic temperature variation becomes stable quickly with the minimum temperature close to the ambient temperature.

Impacts of the operating temperature on the corresponding output voltage and current for the considered convection heat transfer coefficients are shown in Fig. 6b and Fig. 6c. A lower heat transfer coefficient causes higher negative voltages and currents during the heating

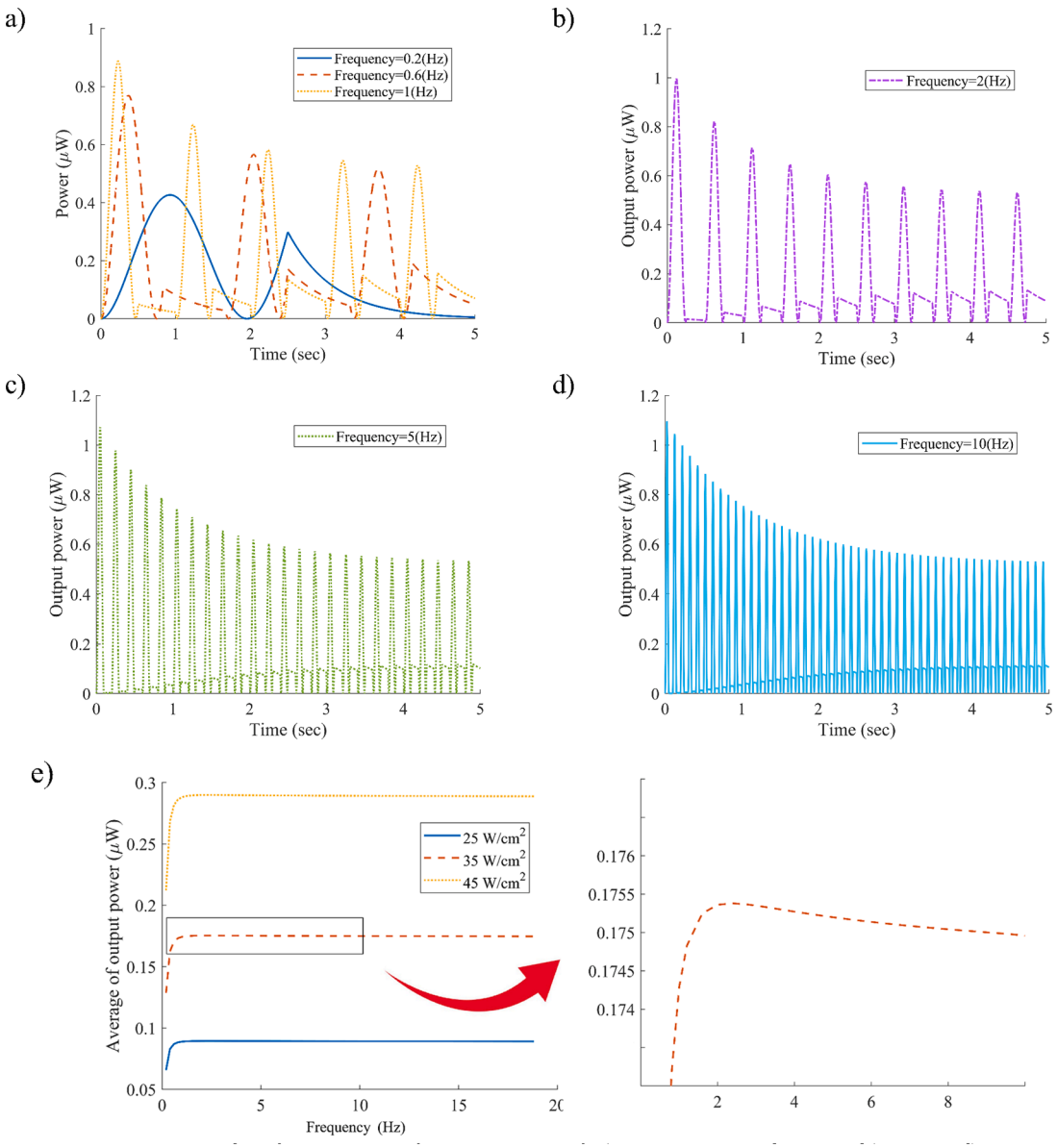


**Fig. 5.** Output power by PEH at frequencies of (a) 0.2, 0.6, and 1 Hz, (b) 5 Hz, (d) 10 Hz, and (e) average output power of PEH at different input heat fluxes during 10 s operating time.

process, while a higher heat transfer coefficient makes higher positive voltages and currents during the cooling process. Comparison of the output voltage and current peak points shows that, an increment in the cooling rate leads to a significant change in the waveform of the generated voltage and current, where another peak point is gained during the cooling process. Decreasing temperature variations under higher heat transfer coefficients result in lower voltage, current, and power generation. Consequently, the heat transfer coefficient is a critical parameter for pyroelectric power generation as illustrated in Fig. 6d.

The average power of PEH under different heat input rates versus different convection heat transfer coefficients is shown in Fig. 7a. Since lower convection heat transfer coefficients result higher temperature variations rate, higher average output power is achievable. Nevertheless, a lower heat transfer coefficient creates a higher operating mean temperature. Thus, the temperature limitations of the power electronic module components and the Curie temperature of the pyroelectric materials must be considered.

External electrical load resistance, furthermore, has a critical influence on PEH conversion performance. Fig. 7b shows the effect of load resistance on the average output power of PEH. There is an optimal load resistance for specific input heat rates to maximize energy harvesting from the pyroelectric material. The peak point of average output power occurs at higher load resistance as the input heat rate increases.

Fig. 8 displays a 3D plot of variations of the average output power as a function of the external load resistance and convection heat transfer coefficient applied to PEH, where the optimal load resistance for the maximum average output power occurs at higher load resistances when the heat transfer coefficient decreases. In order to utilize sufficient electrical power for sensors, a PEH with a larger area can be applied. Alternatively, the energy harvested can be stored and used periodically when the sensor is active.

## 7. Conclusions

In this study, feasibility assessment of PEH used as a DBC substrate of power electronic modules is investigated theoretically. Variations in critical design parameters of PEH system are considered in the form of transient and average power generation. An analytical model is

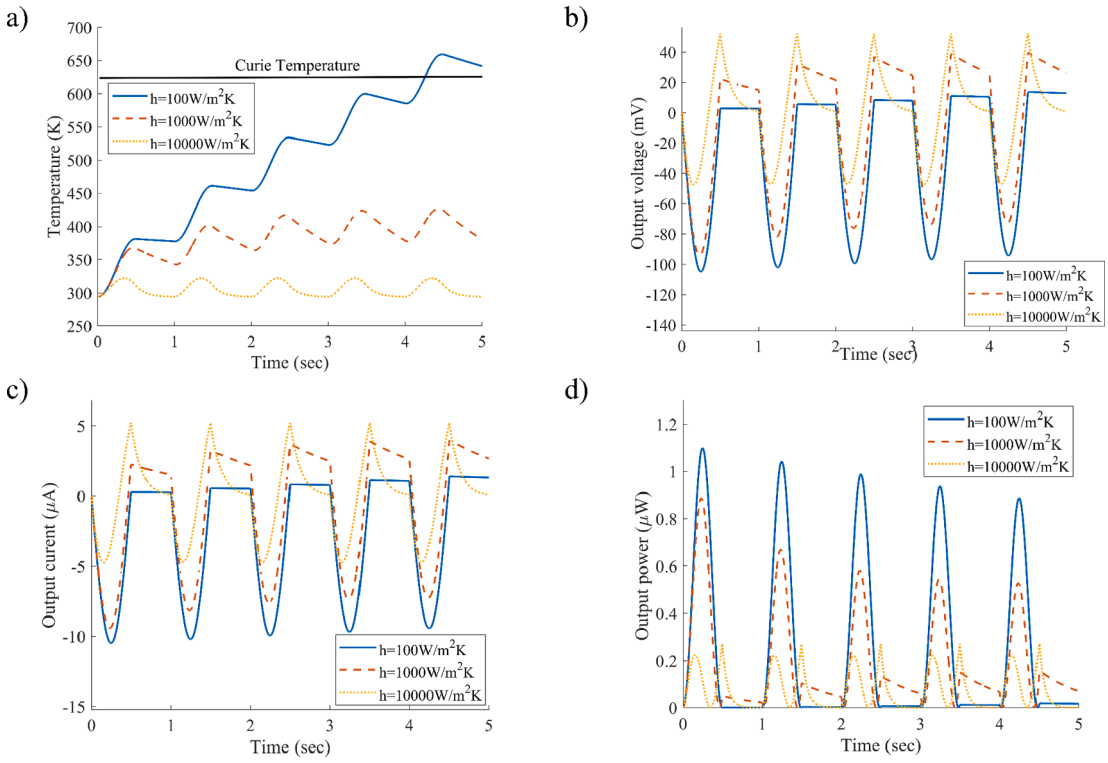


**Fig. 6.** (a) Temperature variation, (b) output voltage, (c) output current, and d) output power of at different heat transfer coefficients on the cold sided of PEH.

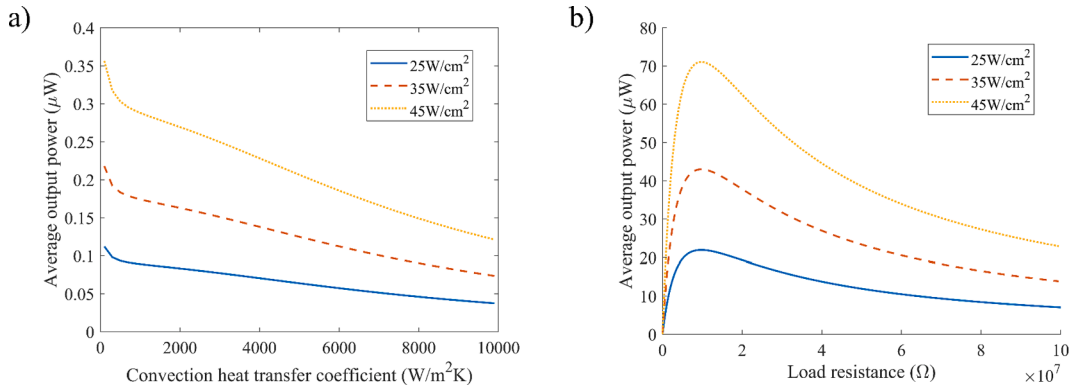


**Fig. 7.** The effect of (a) convection heat transfer coefficient and (b) load resistance on average output power generated by PEH during 10 s operating time.

developed in MATLAB with coupled thermo-pyroelectrical properties of PEH to investigate the impact of the critical parameters on performance of PEH. Results of this study show that the 10 mm × 10 mm × 0.5 mm PEH under half sinusoidal input heat rate with an amplitude of 35 W/cm$^2$, frequency of 1 Hz, and a convection heat transfer coefficient of 1000 W/m$^2$K can harvest average output power of 0.1742 μW. Moreover, the system can harvest 1.7425 μJ during 10 s operation time under these conditions. It is shown that there is a low threshold for the convection heat transfer coefficient to avoid operating at temperatures higher than the Curie temperature. The minimum convection heat transfer coefficient for the proposed PEH module operating under 45 W/cm$^2$ input heat density is 480 W/m$^2$K. The results show that the power generation by the considered PEH can be sufficient for utilization by sensor systems for condition monitoring and wireless data communication applications. This study demonstrates the remarkable potential of PEHs to be used as critical components in power electronic modules as well as an opportunity to provide self-powered and autonomous IIoT systems in a vast range of power electronic applications. To improve performance of PEH system, optimal operating temperature range of PEH for safe operation of the power electronic semiconductor chip and effective energy harvesting close to the Curie temperature, power management of PEH system, and analysis of nonlinearities in the response of the pyroelectric materials to heating and cooling processes can be suggested as future work.

## CRediT authorship contribution statement

**Ali Mohammadnia:** Writing – original draft, Visualization. **Alireza Rezania:** Conceptualization, Methodology, Investigation.

## Declaration of Competing Interest

The authors declare that they have no known competing financial interests or personal relationships that could have appeared to influence the work reported in this paper.

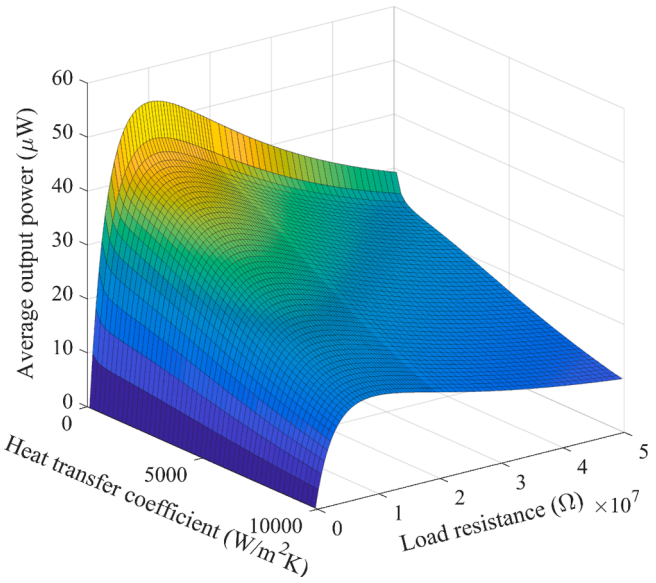


**Fig. 8.** Effect of convection heat transfer coefficient and load resistance on average output power of PEH during 10 s operating time.

## Data availability

Data will be made available on request.

## References


[1] Mohammadnia A, Ziapour BM, Sedaghati F, Rosendahl L, Rezania A. Fan operating condition effect on performance of self- cooling thermoelectric generator system. Energy 2021;224:120177. https://doi.org/10.1016/J.ENERGY.2021.120177.

[2] Mohammadnia A, Rezania A, Ziapour BM, Sedaghati F, Rosendahl L. Hybrid energy harvesting system to maximize power generation from solar energy. Energy Convers Manag 2020;205:112352. https://doi.org/10.1016/j.enconman.2019.112352.

[3] Mohammadnia A, Rezania A. Compatibility assessment of TEGs arrangement coupled with DC/DC converter to harvest electricity from low-temperature heat sources. Energy Conversion and Management: X 2023;18:100356.

[4] Mohammadnia A, Ziapour BM, Sedaghati F, Rosendahl L, Rezania A. Utilizing thermoelectric generator as cavity temperature controller for temperature management in dish-Stirling engine. Appl Therm Eng 2020;165:114568. https://doi.org/10.1016/j.applthermaleng.2019.114568.

[5] Mohammadnia A, Ziapour BM. Investigation effect of a spectral beam splitter on performance of a hybrid CPV/Stirling/TEG solar power system. Appl Therm Eng 2020;180:115799. https://doi.org/10.1016/j.applthermaleng.2020.115799.

[6] Ravindran SKT, Huesgen T, Kroener M, Woias P. A self-sustaining micro thermomechanic-pyroelectric generator. Appl Phys Lett 2011;99(10):104102.

[7] Wang Q, Bowen CR, Lewis R, Chen J, Lei W, Zhang H, et al. Hexagonal boron nitride nanosheets doped pyroelectric ceramic composite for high-performance thermal energy harvesting. Nano Energy 2019;60:144–52.

[8] Patel S, Novak N. The pyroelectric energy harvesting and storage performance around the ferroelectric/antiferroelectric transition in PNZST. J Mater Sci 2021;56:1133–46. https://doi.org/10.1007/S10853-020-05353-4/TABLES/2.

[9] Korkmaz S, Kariper A. Pyroelectric nanogenerators (PyNGs) in converting thermal energy into electrical energy: Fundamentals and current status. Nano Energy 2021;84:105888. https://doi.org/10.1016/J.NANOEN.2021.105888.

[10] Yu C, Park J, Youn JR, Song YS. Sustainable solar energy harvesting using phase change material (PCM) embedded pyroelectric system. Energy Convers Manag 2022;253:115145. https://doi.org/10.1016/J.ENCONMAN.2021.115145.

[11] Wang H, Ng LS, Li H, Lee HK, Han J. Achieving milliwatt level solar-to-pyroelectric energy harvesting via simultaneous boost to photothermal conversion and thermal diffusivity. Nano Energy 2023;108:108184. https://doi.org/10.1016/J.NANOEN.2023.108184.

[12] Yu C, Park J, Ryoun Youn J, Seok SY. Integration of form-stable phase change material into pyroelectric energy harvesting system. Appl Energy 2022;307:118212. https://doi.org/10.1016/J.APENERGY.2021.118212.

[13] Kim J, Yamanaka S, Murayama I, Katou T, Sakamoto T, Kawasaki T, et al. Pyroelectric power generation from the waste heat of automotive exhaust gas. Sustain Energy Fuels 2020;4(3):1143–9.

[14] Xue H, Yang Q, Wang D, Luo W, Wang W, Lin M, et al. A wearable pyroelectric nanogenerator and self-powered breathing sensor. Nano Energy 2017;38:147–54.

[15] Lee J-H, Lee KY, Gupta MK, Kim TY, Lee D-Y, Oh J, et al. Highly Stretchable Piezoelectric-Pyroelectric Hybrid Nanogenerator. Adv Mater 2014;26(5):765–9.

[16] Lee J-H, Ryu H, Kim T-Y, Kwak S-S, Yoon H-J, Kim T-H, et al. Thermally Induced Strain-Coupled Highly Stretchable and Sensitive Pyroelectric Nanogenerators. Adv Energy Mater 2015;5(18):1500704.

[17] Zabek D, Taylor J, Ayel V, Bertin Y, Romestant C, Bowen CR. A novel pyroelectric generator utilising naturally driven temperature fluctuations from oscillating heat pipes for waste heat recovery and thermal energy harvesting. J Appl Phys 2016;120(2):024505.

[18] Raouadi MH, Touayar O. Harvesting wind energy with pyroelectric nanogenerator PNG using the vortex generator mechanism. Sens Actuators A Phys 2018;273:42–8. https://doi.org/10.1016/J.SNA.2018.02.009.

[19] Tabbai Y, Alaoui-Belghiti A, el Moznine R, Belhora F, Hajjaji A, el Ballouti A. Friction and wear performance of disc brake pads and pyroelectric energy harvesting. International Journal of Precision Engineering and Manufacturing - Green Technology 2021;8:487–500. https://doi.org/10.1007/S40684-020-00195-6/TABLES/7.

[20] Lheritier P, Torelló A, Usui T, Nouchokgwe Y, Aravindhan A, Li J, et al. Large harvested energy with non-linear pyroelectric modules. Nature 2022;609(7928):718–21.

[21] Kang M, Yeatman EM. Coupling of piezo- and pyro-electric effects in miniature thermal energy harvesters. Appl Energy 2020;262:114496. https://doi.org/10.1016/J.APENERGY.2020.114496.

[22] Zhang Y, Fan Z, Wen N, Yang S, Li C, Huang H, et al. Novel Wearable Pyrothermoelectric Hybrid Generator for Solar Energy Harvesting. ACS Appl Mater Interfaces 2022;14:17330–9. https://doi.org/10.1021/ACSAMI.2C00874/SUPPL_FILE/AM2C00874_SI_003.MP4.

[23] Ming Hong Ng V, Bing Kong L, Que W, Wang C, Li S, Zhang T. 2.23 Pyroelectric Materials. Comprehensive Energy Systems, Elsevier 2018:720–59. https://doi.org/10.1016/B978-0-12-809597-3.00249-2.

[24] He H, Lu X, Hanc E, Chen C, Zhang H, Lu L. Advances in lead-free pyroelectric materials: a comprehensive review. J Mater Chem C Mater 2020;8:1494–516. https://doi.org/10.1039/C9TC05222D.

[25] Batra AK, Aggarwal MD, Edwards ME, Bhalla A. Present Status of Polymer: Ceramic Composites for Pyroelectric Infrared Detectors. Https://DoiOrg/101080/00150190802363207 2010;366:84–121. https://doi.org/10.1080/00150190802363207.

[26] Kumar A, Kumar S, Patel S, Sharma M, Azad P, Vaish R, et al. Pyroelectric energy conversion using Ba0.85Sr0.15Zr0.1Ti0.9O3 ceramics and its cement-based composites. Https://DoiOrg/101177/1045389X19828491 2019;30(6):869–77.

[27] Ding T, Zhu L, Wang X-Q, Chan KH, Lu X, Cheng Y, et al. Hybrid Photothermal Pyroelectric and Thermogalvanic Generator for Multisituation Low Grade Heat Harvesting. Adv Energy Mater 2018;8(33):1802397.

[28] Li Q, Li S, Pisignano D, Persano L, Yang Y, Su Y. On the evaluation of output voltages for quantifying the performance of pyroelectric energy harvesters. Nano Energy 2021;86:106045. https://doi.org/10.1016/J.NANOEN.2021.106045.

[29] Bowen CR, Taylor J, Leboulbar E, Zabek D, Chauhan A, Vaish R. Pyroelectric materials and devices for energy harvesting applications. Energy Environ Sci 2014;7:3836–56. https://doi.org/10.1039/C4EE01759E.

[30] Ling Bing K, Li T, Hng HH, Boey F, Zhang T, Li S, et al. Waste Energy Harvesting Mechanical and Thermal Energies. Springer; 2014.

[31] OTG-PM - Opsens Industrial n.d. https://opsens-solutions.com/products/fiber-optic-temperature-sensors/otg-pm-fiber-optic-temperature-sensor/ (accessed October 5, 2022).

[32] B2902A Precision Source/Measure Unit, 2 ch, 100 fA, 210 V, 3 A DC/10.5 A Pulse [Discontinued] | Keysight n.d. https://www.keysight.com/dk/en/product/B2902A/precision-source-measure-unit-2-ch-100fa-210v-3a-dc-10-5a-pulse.html (accessed October 5, 2022).

[33] Yousefi E, Nejad AA, Rezania A. Higher power output in thermoelectric generator integrated with phase change material and metal foams under transient boundary condition. Energy 2022;256:124644. https://doi.org/10.1016/J.ENERGY.2022.124644.